

Noncrossing approximation solution of the anisotropic Anderson impurity model

Peter S. Riseborough

Department of Physics, Barton Hall, 1900 N. 13th St., Temple University, Philadelphia, Pennsylvania 19122

(Received 20 February 2002; revised manuscript received 5 August 2002; published 14 January 2003)

The thermodynamic and magnetic properties of a single impurity Anderson model that describes Ce in an environment with hexagonal symmetry is treated within the noncrossing approximation. It is found that the properties of the system at temperatures larger than the crystal field splitting are described by a Kondo temperature of the sixfold-degenerate spin-orbit multiplet and at low temperatures by a highly renormalized Kondo temperature of the crystal field ground state. The inelastic neutron scattering spectra exhibits a quasi-elastic and inelastic component. The results are compared with the concentrated heavy-fermion compound CeAl₃. The system is well described by the single-impurity Anderson model at temperatures above 1 K, with the crystal field scheme determined by Goremychkin *et al.* from inelastic neutron scattering experiments. The excellent agreement may be due to the small variation of the f occupation number with temperature in heavy-fermion systems. However, the single-impurity model fails to describe the peak in the ratio $C(T)/T$ found in earlier experiments. Therefore, it is concluded that this peak is either due to the coherence of the lattice or due to magnetic interactions that may be responsible for spin-glass-like ordering.

DOI: 10.1103/PhysRevB.67.045102

PACS number(s): 71.27.+a

I. INTRODUCTION

The single-impurity Anderson model¹ was developed to describe the properties of transition-metal or rare-earth impurities in a simple metallic host. The model describes both the mechanism whereby local magnetic moments are formed above a characteristic temperature T_k and how these magnetic moments are suppressed and a nonmagnetic (Kondo) singlet state is produced at temperatures lower than T_k . At the lowest temperatures, the solution of the impurity model exhibits a nonmagnetic Fermi-liquid behavior.² However, despite the single-ion character of the physics of the model, the model has also been applied to the description of the physics of concentrated heavy-fermion compounds containing lanthanide and actinide materials that share qualitatively similar properties. The initial reasoning behind the adoption of this description of the concentrated compounds was found in dilution experiments, similar to those first performed by Lin *et al.*³ on CePb₃, where it was observed that the experimentally measured properties scale directly with the concentration of Ce ions. However, similar dilution experiments on CeAl₃ show deviations from the single-impurity Fermi-liquid behavior on increasing the concentration of either the La or Y atoms substituting for Ce.⁴ In particular, the low- T behavior of the electronic specific heat, $C(T)$, shows a sharp peak at a temperature that does not scale with the Kondo temperature as the Ce concentration is varied. This anomalous peak in $C(T)$ also exists in the ordered compound, but is very sample dependent.⁵ It has been suggested that the peak might be due to the RKKY-like interactions that lead to anomalous or frustrated inhomogeneous magnetic ordering in the stoichiometric compound.^{6,7} Alternatively, the deviation from the single-impurity Kondo model may be due to an insufficient number of conduction electrons required to produce a nonmagnetic state for each Ce ion. The theoretical argument about the inapplicability of the single-impurity model to a concentrated compound, due to Nozieres,⁸ is based on the observation that only conduction electrons

within $k_B T_k$ of the Fermi energy $\mu(0)=0$ can be involved in the production of a nonmagnetic (Kondo) singlet. Since each magnetic impurity requires at least one conduction electron to screen its moment, the total number of conduction electrons available for screening the moments is estimated from the conduction band density of states near the Fermi energy, $N_c \rho_c(0)$, as $k_B T_k N_c \rho_c(0)$. The exhaustion argument concludes that, when this number is much less than the number of conduction electrons needed to screen the moment of each f ion in a concentrated compound, the standard Kondo mechanism is unable to screen the local moments. A third possibility, motivated by the observation that the static susceptibility is extremely anisotropic,⁹ is that the discrepancies with the predictions of the single-impurity Anderson model may be partly due to the noncubic crystalline symmetry, which in the limit of almost integer occupation of the f levels results in a Kondo model with an anisotropic Coqblin-Schrieffer interaction.¹⁰ That is, at temperatures above the crystal field splitting the local moment undergoes spin fluctuations between the full $J=\frac{5}{2}$ spin-orbit multiplet which are partially frozen out at temperatures below the crystal field splitting, leading to an anomaly in the specific heat.

Recent low-temperature specific heat measurements⁴ on substitutionally doped Ce_{0.8}La_{0.2}Al₃ also show a pronounced maximum in $C(T)$ near $T=2.3$ K. It has been suggested^{11,12} that these peaks may be described by the anisotropic spin-1/2 Kondo model. However, such peaks only occur for extremely large values of the Ising exchange J_z , i.e., $J_z \rho_c(\mu) > 1$. Furthermore, Pietri *et al.*¹³ have performed numerical renormalization group calculations on the anisotropic Kondo model and have found that the calculated field dependence of $C(T)/T$ is in disagreement with the experimentally determined behavior.

In this paper, we examine the properties of the single-impurity Anderson model as calculated using the noncrossing approximation (NCA),¹⁴⁻¹⁶ in the presence of crystalline anisotropy, for nonscaling behavior. We shall use this to examine the effects of both the anisotropy and crystal field

splittings on the properties of pure CeAl₃. In particular, we shall examine the specific heat, susceptibility, and inelastic neutron scattering spectra.

II. CRYSTALLINE SYMMETRY AND IMPURITY MODEL

We shall consider the Anderson impurity in the presence of a hexagonal crystalline field. The crystalline electric field raises the symmetry of the sixfold-degenerate low-lying f electron $J = \frac{5}{2}$ multiplet into three groups of crystalline field levels.¹⁷ With the ideal hexagonal c/a ratio, the crystal field splits the sixfold-degenerate ground-state multiplet into the three crystal field doublets $|\Gamma_7\rangle = |\pm \frac{1}{2}\rangle$, $|\Gamma_8\rangle = |\pm \frac{5}{2}\rangle$, and $|\Gamma_9\rangle = |\pm \frac{3}{2}\rangle$ with energies $2\Delta E$, ΔE , and $-3\Delta E$, respectively. Analyses of inelastic neutron scattering experiments^{18,11} suggest that the crystal field splitting parameter is given by $\Delta E \approx 1.5$ meV. On using the Coqblin-Schrieffer formalism,¹⁰ one expects that the Kondo exchange interaction should also be anisotropic and produce an anisotropic Kondo effect.

The model Hamiltonian is given by the sum of three terms as follows:

$$\hat{H} = \hat{H}_f + \hat{H}_c + \hat{H}_{fc}. \quad (1)$$

The first term \hat{H}_f represents the energy of the electrons in the localized f orbits of the Ce ion. The second term \hat{H}_c represents the energy of (noninteracting) electrons in the conduction-band states. The third term \hat{H}_{fc} represents the hybridization or coupling between the conduction band and localized f states. The energy \hat{H}_f is given as a sum of the binding energy $E_f(\alpha)$, which is spin-orbit and crystal field split, and a screened Coulomb interaction of strength U acting between pairs of electrons. The operator \hat{H}_f can be written as

$$\hat{H}_f = \sum_{\alpha} E_f(\alpha) f_{\alpha}^{\dagger} f_{\alpha} + \sum_{\alpha, \beta} \frac{U}{2} f_{\alpha}^{\dagger} f_{\beta}^{\dagger} f_{\beta} f_{\alpha}, \quad (2)$$

in which f_{α}^{\dagger} and f_{α} , respectively, create and annihilate an electron in the one electron f orbital labeled by the combined crystal field and spin-orbit quantum number α . In the following, we shall assume that U is the largest energy in the problem and take the limit $U \rightarrow \infty$, thereby projecting out states in which the f orbital is occupied by two or more electrons. The conduction-band Hamiltonian \hat{H}_c is expressed as the sum of the energies of the electrons in the Bloch states,

$$\hat{H}_c = \sum_{\underline{k}, \alpha} \varepsilon(\underline{k}, \alpha) c_{\underline{k}, \alpha}^{\dagger} c_{\underline{k}, \alpha}, \quad (3)$$

where $\varepsilon(\underline{k}, \alpha)$ is the Bloch energy of an electron with Bloch wave vector \underline{k} in the subband labeled by α . The creation and annihilation operators for an electron in the Bloch state (\underline{k}, α) , respectively, are denoted by $c_{\underline{k}, \alpha}^{\dagger}$ and $c_{\underline{k}, \alpha}$. The hybridization term \hat{H}_{fc} is written as

$$\hat{H}_{fc} = \frac{1}{\sqrt{N}} \sum_{\underline{k}, \alpha} [V_{\alpha}(\underline{k}) f_{\underline{k}, \alpha}^{\dagger} c_{\underline{k}, \alpha} + V_{\alpha}^*(\underline{k}) c_{\underline{k}, \alpha}^{\dagger} f_{\underline{k}, \alpha}], \quad (4)$$

in which the first term represents a process whereby a conduction electron tunnels into the f orbital through the centrifugal barrier and the Hermitian conjugate represents the time-reversed process. The combined spin-orbit and crystal field index is conserved in the tunneling process, corresponding to conservation of combined spin and orbital angular momenta.

III. NCA CALCULATION

We solve the $U \rightarrow \infty$ limit of the Anderson impurity Hamiltonian within the NCA, using a Gaussian model for the bare (nonhybridized) conduction-band density of states. The density of states per site, $\rho_{\alpha}(\varepsilon)$, for the α th conduction subband are assumed to all be degenerate and are given by

$$\rho_{\alpha}(\varepsilon) = \frac{1}{N} \sum_{\underline{k}} \delta(\varepsilon - \varepsilon(\underline{k}, \alpha)) = \frac{1}{W\sqrt{\pi}} \exp\left[-\left(\frac{\varepsilon}{W}\right)^2\right], \quad (5)$$

which has a half-width of W . From off-resonance valence-band photoemission and bremsstrahlung isochromat spectroscopy (BIS) experiments, one can estimate that the conduction-band density of states of Ce has a half-width of $W = 3$ eV. From photoemission experiments, one estimates that the position of the bare f level is located about -2 eV below the Fermi energy. Accordingly, we set $E_f(\Gamma_9) = -2$ eV and that the crystal field excited states have energies of $E_f(\Gamma_8) = -1.994$ eV and $E_f(\Gamma_7) = -1.9925$ eV. The eightfold-degenerate, $N_{s-o} = 8$, $J = \frac{7}{2}$ excited spin-orbit split f -level energy is located above the ground-state f -level energy by the free-atom spin-orbit splitting (0.27 eV), so we set $E_f(s-o) = -1.63$ eV. The hybridization matrix element V is assumed to be independent of (\underline{k}, α) and the magnitude was adjusted to yield the best fit with the inelastic neutron scattering data on CeAl₃ taken at $T = 40$ K.

In the limit of infinite U , the f states of multiple occupancy are projected out in the initial, final, and all intermediate states. Thus, the states can be characterized as having either an unoccupied or a singly occupied f shell. The NCA equations are obtained from perturbation theory in the hybridization matrix element by selectively summing a subset of diagrams which yield an exact expression for the self-energy to order $1/N_f$, where N_f is the degeneracy of the f level.¹⁴⁻¹⁶ The subset of diagrams are those which neglect all vertex corrections. The NCA equations are expressed as the coupled nonlinear integral equations for the unoccupied and occupied f level self-energies¹⁹ which are, respectively, denoted by $\Sigma_0(\omega)$ and $\Sigma_{\alpha}(\omega)$. The integral equations have the form

$$\Sigma_{\alpha}(\omega + i\delta) = \frac{1}{N} \sum_{\underline{k}} \frac{|V_{\alpha}(\underline{k})|^2 [1 - f(\varepsilon(\underline{k}, \alpha))]}{\omega - \varepsilon(\underline{k}, \alpha) + i\delta - \Sigma_0[\omega - \varepsilon(\underline{k}, \alpha) + i\delta]} \quad (6)$$

and

$$\begin{aligned} \Sigma_0(\omega + i\delta) & \frac{1}{N} \\ & = \sum_{\underline{k}, \alpha} \frac{|V_\alpha(\underline{k})|^2 f(\varepsilon(\underline{k}, \alpha))}{\omega + \varepsilon(\underline{k}, \alpha) + i\delta - E_f(\alpha) - \Sigma_\alpha[\omega + \varepsilon(\underline{k}, \alpha) + i\delta]}, \end{aligned} \quad (7)$$

where $f(x)$ is the Fermi-Dirac distribution function and the sum over α runs over all the individual f states. These equations are solved numerically. The behavior of the real and imaginary parts of the empty f -state self-energy $\Sigma_0(\omega)$ are shown in Fig. 1(a), for $T=10$ K. The imaginary part of the self-energy falls to almost zero near $\omega E_f(\Gamma_7)$ due to the cutoff originating in the Fermi function. The real part of the self-energy shows evidence of the Kondo resonance near the same energy. The logarithmic divergence in the real part, expected from perturbation theory in powers of V , is suppressed partially by the thermal broadening due to the Fermi function and also partially by the smearing due to the finite imaginary part of the occupied-state self-energy. As a result of thermal smearing, structures associated with the crystal field split Kondo resonances are not resolved at $T=10$ K, but can be clearly observed at $T=0.5$ K. However, at 10 K, the real and imaginary parts of the empty-state self-energy do show structure originating from the spin-orbit split excited-state Kondo resonance at an energy of roughly 0.27 eV above the ground-state resonance. The real and imaginary parts of the occupied f -state self-energies $\Sigma_\alpha(\omega)$ are shown in Fig. 1(b). For energies far removed from those associated with the Kondo resonance, the occupied-state self-energy is a factor of 14 smaller than the unoccupied-state self-energy. Furthermore, $\Sigma_\alpha(\omega)$ does not show features as sharp as those in the unoccupied-state self-energy.

To improve the numerical accuracy, a similar pair of linearized equations are also solved (up to a multiplicative constant) self-consistently for the Boltzmann weighted imaginary part of the self-energies,

$$\eta_\alpha(\omega + i\delta) = \frac{1}{\pi} \frac{\exp[-\beta\omega]}{Z_f} \text{Im}[\Sigma_\alpha(\omega + i\delta)] \quad (8)$$

and

$$\eta_0(\omega + i\delta) = \frac{1}{\pi} \frac{\exp[-\beta\omega]}{Z_f} \text{Im}[\Sigma_0(\omega + i\delta)], \quad (9)$$

in which the previously found self-energies form part of the input.

The partition function for the f electrons, Z_f , is calculated in a processes which commences with the construction of the occupied- and unoccupied-state densities $\rho_\alpha(\omega)$ and $\rho_0(\omega)$ defined by

$$\begin{aligned} \rho_\alpha(\omega) & = -\frac{1}{\pi} \\ & \times \frac{\text{Im}[\Sigma_\alpha(\omega + i\delta)]}{\{\omega - E_f(\alpha) - \text{Re}[\Sigma_\alpha(\omega)]\}^2 + \{\text{Im}[\Sigma_\alpha(\omega + i\delta)]\}^2}, \end{aligned} \quad (10)$$

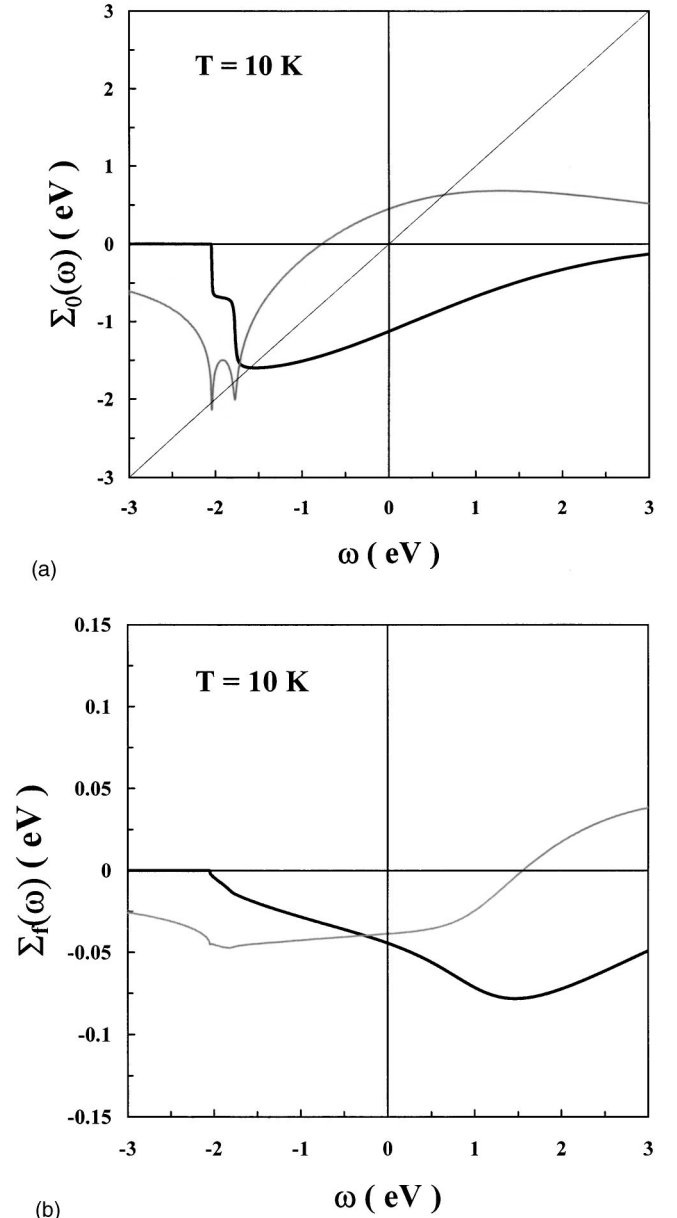


FIG. 1. The energy dependence of the real and imaginary parts of the unoccupied-state self-energy $\Sigma_0(\omega)$ is shown in (a) by the thin and thick solid lines. The energy of the Kondo bound states is given by the intersection of the dotted line, ω , passing through the origin with the real part of the unoccupied-state self-energy. At $T = 10$ K, the system supports a bound state corresponding to the ground-state $J = \frac{5}{2}$ spin-orbit split f level and also a second Kondo bound state corresponding to the $J = \frac{7}{2}$ spin-orbit excited f state. The real and imaginary parts of the lowest-energy occupied-state self-energy $\Sigma_\alpha(\omega)$ are shown in (b), as thin and thick solid lines. The occupied-state self-energy has a magnitude which is a factor of N_f smaller than the unoccupied self-energy.

$$\rho_0(\omega) = -\frac{1}{\pi} \frac{\text{Im}[\Sigma_0(\omega + i\delta)]}{\{\omega - \text{Re}[\Sigma_0(\omega)]\}^2 + \{\text{Im}[\Sigma_0(\omega + i\delta)]\}^2}. \quad (11)$$

The occupied- and unoccupied-state densities of states are shown in Fig. 2(a) over a wide energy scale. The unoccupied

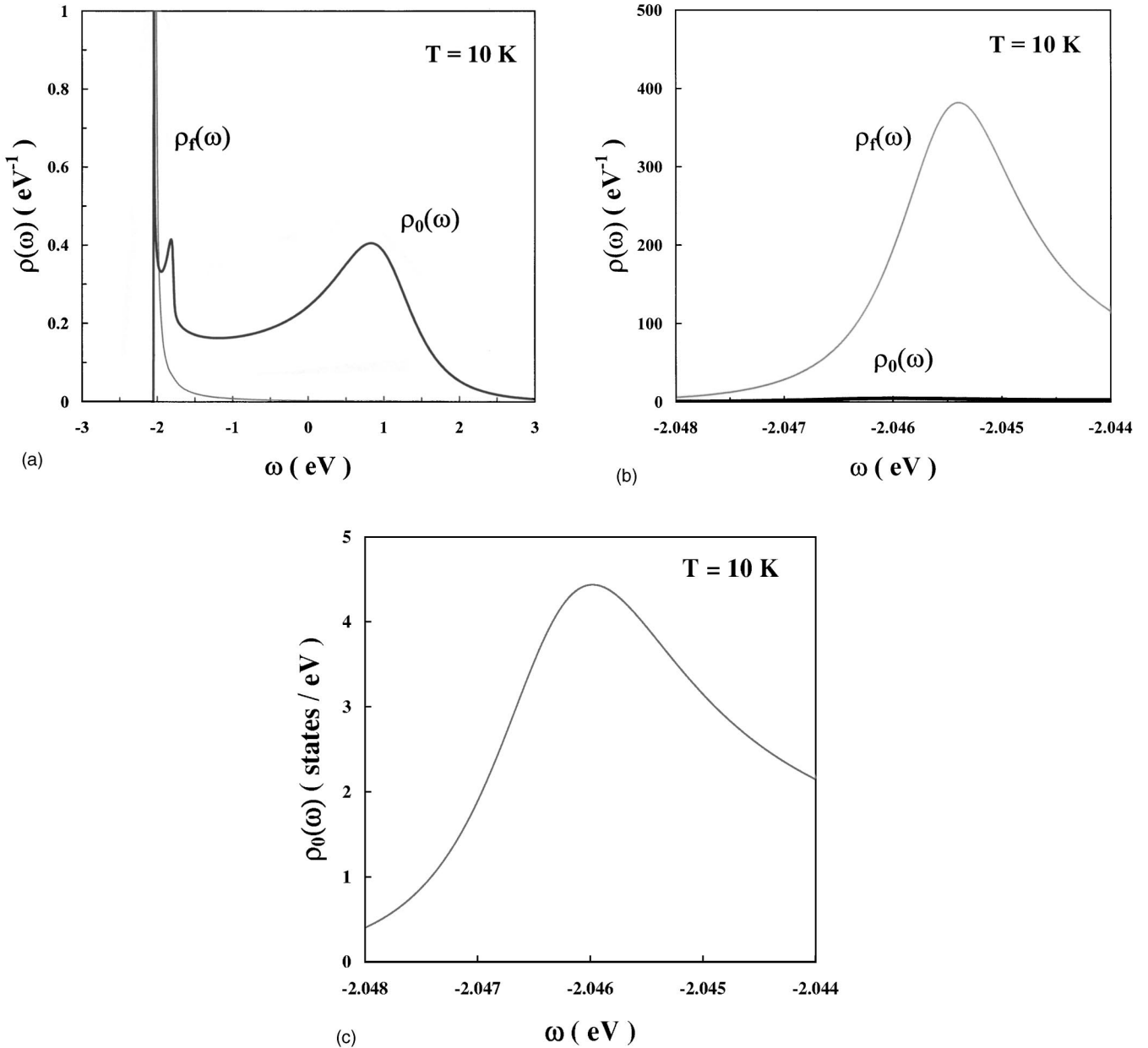


FIG. 2. The lowest-energy occupied- and unoccupied-state densities of states $\rho_\alpha(\omega)$ and $\rho_0(\omega)$ are shown in (a) by thin and thick solid lines. The densities of states are in units of $\text{eV}^{-1} (\text{mol Ce})^{-1}$, and the energy ω is in units of eV. The unoccupied-state density of states exhibits three peaks, two of which correspond to the Kondo bound states of the $J = \frac{5}{2}$ and $J = \frac{7}{2}$ spin-orbit multiplets. The occupied-state density of states only shows a single peak close to the energy of the lowest-energy Kondo bound state. The low-energy structure is shown in more detail in (b). The lowest-energy peak in the unoccupied density of states lies at an energy approximately $k_B T_K^*$ below the peak in the occupied density of states. The structure in the spectral density $\rho_0(\omega)$ is barely discernable in (b) and, therefore, is shown in (c) with a scale that has been magnified by a factor of 100.

density of states shows three peaks associated with the solutions of the equation

$$\omega - \text{Re}[\Sigma_0(\omega)] = 0. \quad (12)$$

The two low-energy peaks in the unoccupied density of states are associated with $J = \frac{5}{2}$ and $J = \frac{7}{2}$ spin-orbit split Kondo peaks. The occupied density of states also shows a sharp peak close to E_f . Near the thermally smeared threshold for the imaginary part of the unoccupied self-energy, the

rapid variation in the real part of the self-energy produces a dramatic narrowing of the low-energy peaks. The structure near the thermally smeared threshold is shown in Fig. 2(b). The peak in the unoccupied density of states lies at an energy $k_B T_K^*$ below the peak in the occupied density of states. The process of evaluating Z_f is continued by the construction of the Boltzmann weighted densities, defined by

$$\Pi_\alpha(\omega) = \frac{\exp[-\beta\omega]}{Z_f} \rho_\alpha(\omega) \quad (13)$$

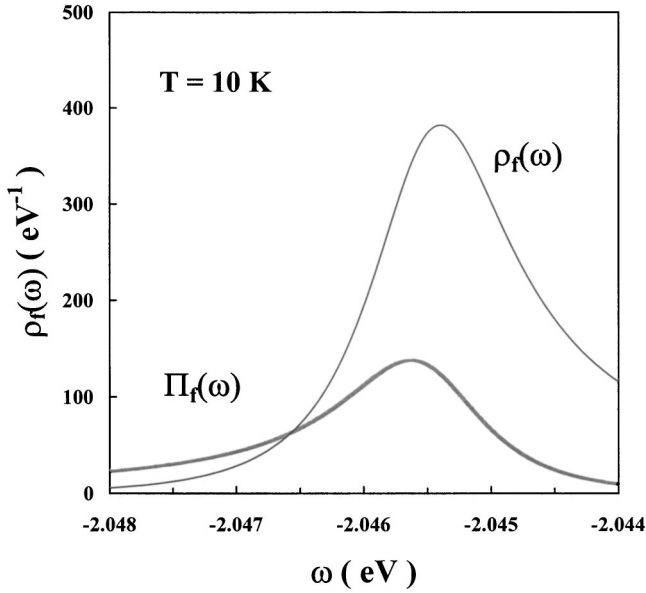


FIG. 3. The thermally weighted occupied-state density of states $\Pi_\alpha(\omega)$ is shown by a thick solid line, while the unweighted occupied-state density of states $\rho_\alpha(\omega)$ is shown by a thin solid line for $T = 10$ K. The units are the same as those in Fig. 2. The thermal weighting factor shifts the spectral weight to lower energies.

and

$$\Pi_0(\omega) = \frac{\exp[-\beta\omega]}{Z_f} \rho_0(\omega). \quad (14)$$

As seen in Fig. 3, at low temperatures, due to the Boltzmann factor, the thermally weighted densities contain a significant amount of their spectral weight at energies far below the low-energy peaks in $\rho_\alpha(\omega)$. In order to avoid amplification of the numerical errors in $\rho_\alpha(\omega)$ in the region where it is small, the weighted densities of states $\Pi_\alpha(\omega)$ are calculated directly from the Boltzmann weighted imaginary parts of the self-energies $\eta_\alpha(\omega)$. The value of the f -electron partition function Z_f is then calculated by imposing the normalization condition

$$1 = \int_{-\infty}^{\infty} d\omega \Pi_0(\omega) + \sum_{\alpha} \int_{-\infty}^{\infty} d\omega \Pi_{\alpha}(\omega). \quad (15)$$

The specific heat due to the impurity is calculated from the impurity partition function Z_f in the usual way. The specific heat contribution $C(T)$ due to each Ce impurity is given by

$$C(T) = -T \left(\frac{\partial^2 F_f(T)}{\partial T^2} \right)_{\mu=0}, \quad (16)$$

since we have assumed a symmetric conduction-band density of states. The temperature-dependent f -electron occupation number is then calculated from

$$n_f(T) = \sum_{\alpha} \int_{-\infty}^{\infty} d\omega \Pi_{\alpha}(\omega). \quad (17)$$

The imaginary part of the dynamic susceptibility $\chi^{\gamma,\delta}(\omega)$ is calculated from the expression

$$\begin{aligned} & (g\mu_B)^{-2} [1 + N(\omega)] \text{Im}[\chi^{\gamma,\delta}(\omega)] \\ &= \pi \sum_{(\alpha,\mu),(\alpha',\mu')} \langle \alpha,\mu | J^{\gamma} | \alpha',\mu' \rangle \langle \alpha',\mu' | J^{\delta} | \alpha,\mu \rangle \\ & \times \int_{-\infty}^{\infty} d\varepsilon \Pi_{\alpha}(\varepsilon) \rho_{\alpha'}(\varepsilon + \omega), \end{aligned} \quad (18)$$

in which $N(\omega)$ is the Bose-Einstein distribution function. In the above expression, we have ignored the effect of excitations from the ground state to the excited spin-orbit level as we have only considered excitations between states with the same J values. However, these excitations can be incorporated by introducing the dipole matrix elements calculated by Balcar and Lovesey.²⁰ The peaks found from the spin-orbit excitations are at higher energies than the energy region of interest here, have small intensities, and are quite broad. The static susceptibility is calculated directly from the occupied-state spectral densities $\rho_{\alpha}(\varepsilon)$ and $\Pi_{\alpha}(\varepsilon)$ in a manner physically equivalent to imposing the Kramers-Kronig relation^{16,19}

$$\chi^{\gamma,\gamma}(T) = \frac{2}{\pi} \int_0^{\infty} d\omega \left(\frac{\text{Im}[\chi^{\gamma,\gamma}(\omega)]}{\omega} \right). \quad (19)$$

The effect of neglecting the spin-orbit excitations is found to be about only 1% of the total susceptibility. On completely neglecting the effects of states other than those in the $J = \frac{5}{2}$ spin-orbit multiplet, we find that our results satisfy the sum rule

$$\begin{aligned} & (g\mu_B)^{-2} \int_{-\infty}^{\infty} \frac{d\omega}{\pi} [1 + N(\omega)] \sum_{\gamma} \text{Im}[\chi^{\gamma,\gamma}(\omega)] \\ &= J(J+1) n_f(T). \end{aligned} \quad (20)$$

However, due to the relatively small value of the spin-orbit splitting in Ce compared to V, and the effects of finite U , it is not expected that this sum rule should hold for the experimental data.

IV. DISCUSSION

The dynamic susceptibility of the single-impurity Anderson model, as calculated by the NCA, was fitted to inelastic neutron scattering experiments on CeAl₃ at 40 K and the measured static susceptibility at one (high-) temperature value. The best fit parameter for the hybridization seems to be $V = 0.45$ eV, which yields an almost integer value for the low-temperature f occupation, $n_f(T = 5 \text{ K}) = 0.9611$. The calculated spectra for spin fluctuations parallel and perpendicular to the hexagonal c axis are shown in Fig. 4. The sum should be compared with the experimentally measured spectrum.^{18,11} We note that there is fair agreement; however, the experimentally determined high-energy tail of the spectrum is larger than the calculated tail. In Fig. 4(a), the spectra are shown for the temperature $T = 20$ K, while in Fig. 4(b), the spectra are shown for $T = 40$ K. The width $\Gamma(T)$ of the quasielastic component [or more precisely the peak position

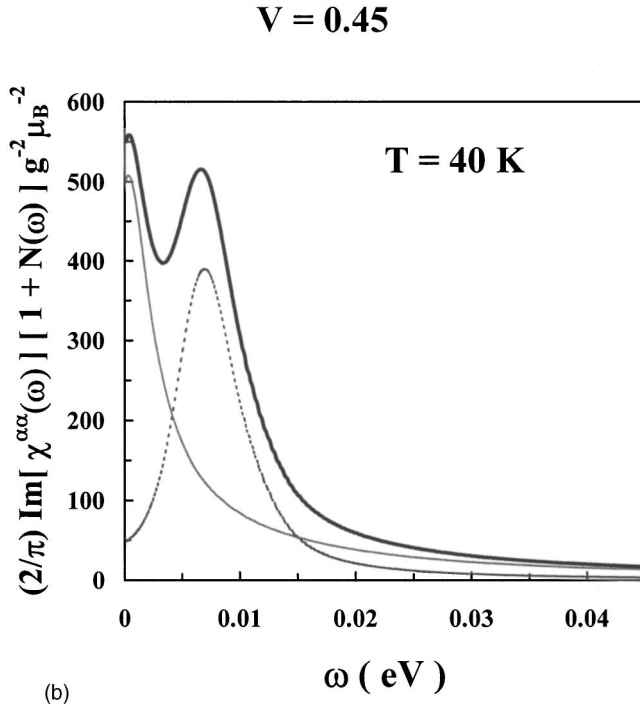
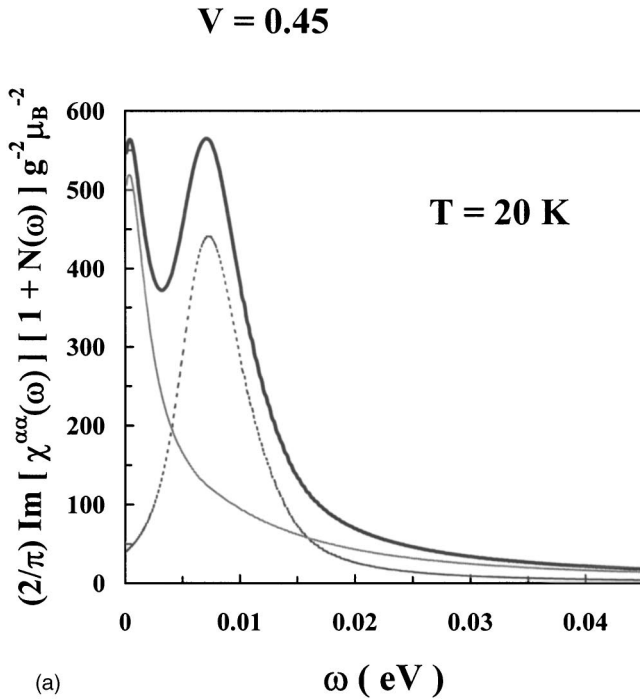


FIG. 4. The thermally weighted dynamic susceptibility in units of $\text{eV}^{-1} (\text{mol Ce})^{-1}$, corresponding to the inelastic neutron scattering and quasielastic neutron scattering spectra, respectively, is shown by the dashed and thin solid lines. The sum is shown by the thick solid lines. The spectra are shown for $T=20$ K in (a) and in (b) for $T=40$ K.

of $\text{Im} \chi^{z,z}(\omega)$ is comparable to that measured by Murani *et al.*²¹ and shows a characteristic

$$\Gamma(T) = \Gamma(0) + B\sqrt{T} \quad (21)$$

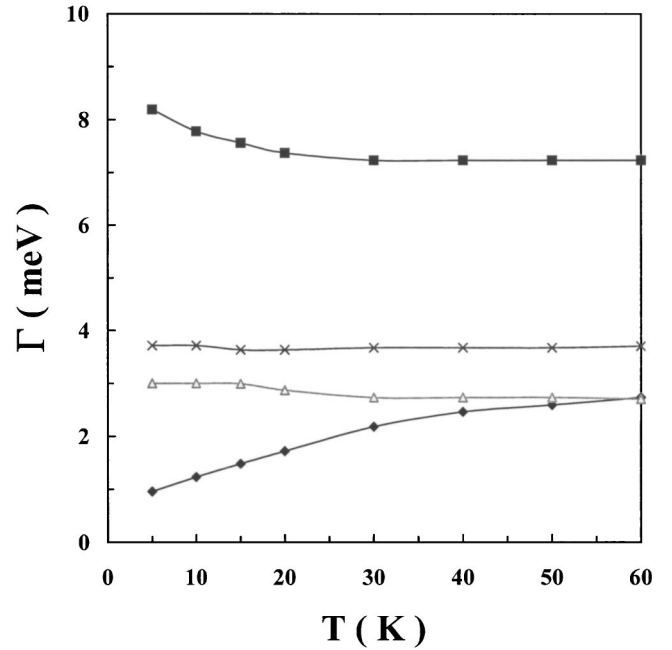


FIG. 5. The temperature dependence of the energy of the quasielastic peak $\Gamma(T)$ in $\text{Im} \chi^{z,z}(\omega)$ is shown by the diamonds. This follows an approximate square-root temperature dependence first seen in CeAl_3 by Murani *et al.* (Ref. 21) and later found in the single-impurity Anderson model calculations of Bickers *et al.* (Ref. 16). The energy of the inelastic peak is marked by the solid squares and softens with increasing temperature. This softening is a result of the reduction of the effective hybridization caused by the change of $n_f(T)$ with temperature which reduces the large hybridization induced renormalization of the crystal field energies. The low-energy-side half width at half maximum of the inelastic peak is shown by the crosses while the high-energy-side half width at half maximum is shown by the triangles.

temperature dependence, as seen in Fig. 5. The energy of the inelastic peak in $\text{Im} \chi^{x,x}(\omega)$ softens as T is increased. This softening occurs over the same temperature range over which $n_f(T)$ changes. Since the hybridization increases the crystal field parameters of CeAl_3 over the values found in similar rare-earth compounds,^{18,22} this softening may be attributable to the reduction of the effective hybridization $V^2[1 - n_f(T)]$ with increasing temperature. In contrast to the temperature dependence of the quasielastic peak, the half widths at half maximum of the inelastic component are relatively temperature independent. The half widths of the inelastic peak are almost equal, indicating the almost symmetric nature of the peak due to the crystal field excitations. The calculated components of the static susceptibility are shown in Fig. 6. The calculated susceptibility tensor shows slightly less anisotropy than the measured quantities.⁹ This discrepancy might be due to anisotropy in the hybridization matrix elements or perhaps deviation from the perfect hexagonal c/a ratio. The temperature dependence of the ratio of the calculated electronic specific heat, $C(T)$, is shown in Fig. 7. At zero field, the specific heat shows a shoulder near $T=6$ K which is due to the Kondo doublet, and a Schottky peak near $T=28$ K, which is due to the crystal field excitations. It is notable that while theory only shows a monotonic

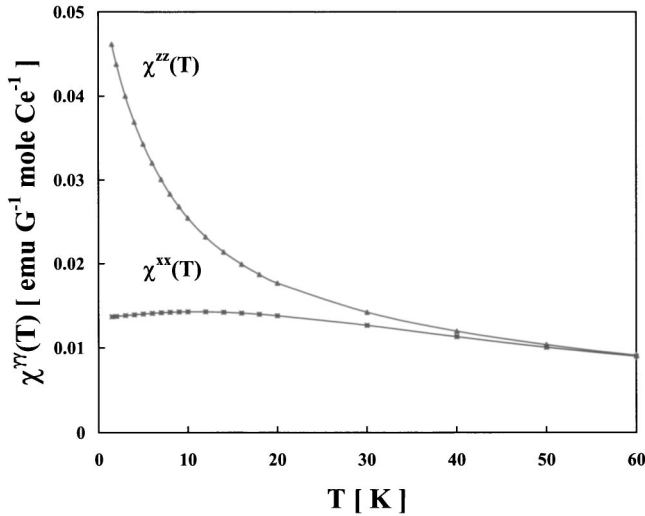


FIG. 6. The temperature dependence of the diagonal components of the static susceptibility, $\chi^{\gamma\gamma}(T)$. The susceptibility is in units of emu per gauss per mole Ce. The $\chi^{z,z}$ component is marked by solid triangles, whereas the $\chi^{x,x}$ and $\chi^{y,y}$ components are degenerate and are marked by solid squares.

increase in the $C(T)/T$ ratio, the measured specific heat ratio shows a maximum of about 1.63 J/mol K^2 , at about $T = 10.5 \text{ K}$, and is followed by a saturation at $T=0$ to a value of 1.5 J/mol K^2 .

The reasonable agreement of both the temperature dependence of thermodynamic quantities and the energy dependence of spectra measured in heavy-fermion systems with the predictions of the single-impurity model is in contrast

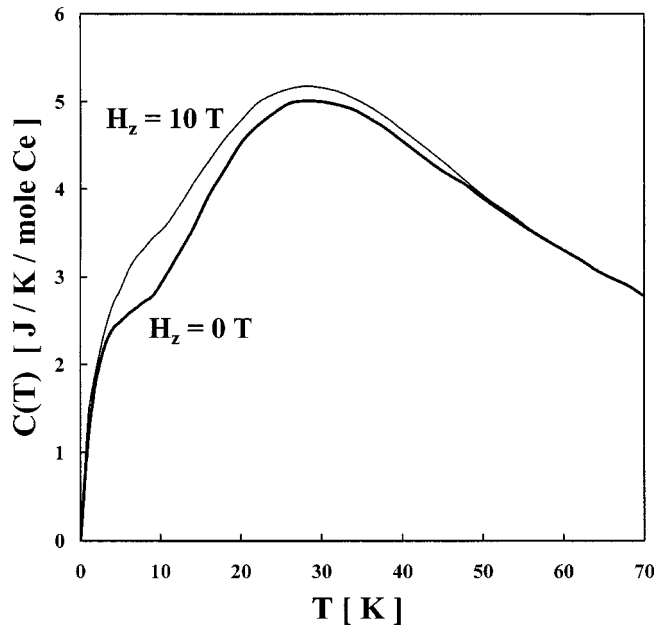


FIG. 7. The temperature dependence of the calculated electronic specific heat, $C(T)$, is shown for $H_z=0$ and $H_z=10 \text{ T}$. The calculation shows a Schottky peak at $T=28 \text{ K}$ and a low-temperature shoulder due to Kondo scattering. The calculation does not reproduce the experimentally determined peak in the specific heat ratio found at temperatures near $T \sim 1 \text{ K}$.

with the marked discrepancy found in the case of Yb mixed-valent compounds.²³ In highly mixed-valent systems it is found that the temperature variation of thermodynamic functions is much slower than the predictions of the single-impurity model. A similar change in the temperature variation between the single-impurity model and the Anderson lattice has been found in Monte Carlo calculations.²⁴ The protracted screening found in the lattice systems is partially due to the necessity of calculating the chemical potential $\mu(T)$ self-consistently. The reasonable agreement of the temperature dependence of experimental measurements on heavy-fermion systems with the single-impurity model may, in part, be due to the very limited change of the f occupation from the low-temperature value to the high-temperature value of unity. This implies that for a concentrated compound, the chemical potential should decrease by an energy of the order of $(W/N_c)[1-n_f(0)]$ for a temperature change of the order of several T_k . In this expression, N_c is the total degeneracy of the conduction bands in the vicinity of the Fermi energy, and not just the number involved in screening the high-temperature magnetic moments. The decrease in the ground-state energy on increasing temperature, due to the shift in the chemical potential, may partially offset the increase in the energy caused by the unbinding of the Kondo singlet state. This competition may result in the slower temperature dependence of thermodynamic quantities in a concentrated compound than in a dilute alloy, where the shift of the chemical potential can be neglected. For the concentrated compound CeAl_3 , the shift of chemical potential is estimated to be of the order of 25 meV , whereas the binding energy $k_B T_k$ for forming the Kondo singlet is estimated to be of the order of $6[1-n_f(0)]V^2\rho_c(0) \sim 8.8 \text{ meV}$.

Using the parameters obtained in the fit, the temperature dependence of the components of the susceptibility and specific heat are in overall reasonable agreement with the single-impurity calculations for temperatures above a few degrees kelvin. In particular, the results show that the model exhibits two different many-body temperature scales; one scale is associated with the Kondo temperature T_k of the full sixfold-degenerate f level. It is this scale that characterizes the spin-flip scattering in the high-temperature regime where the excited crystal field levels are thermally populated. For temperatures below the crystal field splitting, where spin-flip scattering between the excited crystal field levels is frozen out, the relevant many-body temperature scale is the Kondo temperature T_k^* of with the doubly degenerate crystal field ground state. The existence of these two temperature scales was first identified by Cornut and Coqblin²⁵ in their explanation of two different temperature regimes of the logarithmic dependences of the resistivity on temperature for dilute Ce impurities. The value of T_k is estimated by resumming low-order perturbation series as

$$k_B T_k \sim W[V^2\rho_c^2(0)]^{1/6} \left(\frac{W}{\Delta E_{s-o}}\right)^{8/6} \exp\left[\frac{E_f}{6V^2\rho_c(0)}\right], \quad (22)$$

which yields $T_k \sim 60 \text{ K}$, which should be compared with the temperatures of 70 and 87 K which correspond to the crystal

field excitation energies. The high-temperature Kondo scale appears as a Curie-Weiss-like term in the asymptotic form of the susceptibility,

$$\chi(T) = \chi^0(T) \left(1 - \frac{2}{N \ln(T/T_k)} + \dots \right), \quad (23)$$

where $\chi^0(T)$ is the susceptibility of an isolated f ion. In the crystal field analysis of the high-temperature susceptibility,¹⁸ the Kondo temperature term is partially incorporated as a mean-field enhancement factor. The lower-temperature scale T_k^* is estimated to be

$$k_B T_k^* \sim W [V^2 \rho_c^2(0)]^{1/2} \left(\frac{W^2}{20 \Delta E^2} \right) \left(\frac{W}{\Delta E_{s-o}} \right)^4 \exp \left[\frac{E_f}{2 V^2 \rho_c(0)} \right]. \quad (24)$$

The above estimate for the low-temperature Kondo temperature T_k^* is not expected to be accurate as the parameters of the low-temperature model are expected to be highly renormalized by the hybridization with the higher-energy levels. A more accurate value of the low-temperature scale T_k^* is given by defining $k_B T_k^*$ as the extrapolated $T \rightarrow 0$ limit of the energy of the peak of either the Kondo feature in the joint f -derived photoemission and inverse photoemission spectrum or the quasielastic peak in $\text{Im} \chi^{z,z}(\omega)$. Thus, a more accurate estimate of the low-temperature energy scale is given by $T_k^* \sim 5.2$ K. This second Kondo temperature T_k^* is expected to show up as the energy scale for the low-temperature Fermi liquid.² However, as shown by Kuramoto and Müller-Hartmann,¹⁵ the NCA solution exhibits spurious behavior for temperatures

$$k_B T < \left(\frac{k_B T_k^*}{N^* + 1} \right) \left(\frac{\pi k_B T_k^*}{V^2 \rho_c(0)} \right)^{(N^* + 1)/(N^* - 1)}, \quad (25)$$

which prevents the Fermi-liquid relations from being completely fulfilled.

Despite the overall reasonable agreement, we find that the peak in the low-temperature specific heat near 1 K in the stoichiometric compound,⁵ or near 3 K (Ref. 4) in the diluted compound, is not well described by the single-impurity model. Although we do find a low-temperature shoulder to the Schottky peak in $C(T)$, the magnitude is considerably smaller than the experimentally determined peak, and the

temperature of the maximum is an order of magnitude higher than the experimentally determined temperature. The field dependence of the calculated low-temperature feature in $C(T)$ shows, as expected, that application of a magnetic field suppresses the Kondo effect and, therefore, reduces the coefficient γ of the linear- T term in the low-temperature specific heat. Furthermore, the Zeeman splitting broadens the shoulder and moves it towards higher temperatures. Although these results are qualitatively similar to those found by Pietri *et al.* using the anisotropic Kondo model,¹³ in our results, the magnitude of the peak is significantly weaker and are almost masked by the Schottky anomaly due to the crystal field splitting. This is partially due to the difference in the model and also as our parameters correspond to a much weaker value of the exchange interaction. Therefore, we conclude, like previous authors,^{4,13} that the existence of a large peak at this very low temperature is a manifestation of the onset of spatial coherence between the f ions. The present calculations contain no indication of whether this is a coherence effect associated with a paramagnetic ground state or whether the anomaly is due to weak, sample-dependent, magnetic ordering found in some experiments. However, it is interesting to note that this peak appears at a temperature of roughly T_k^*/N^* where N^* is the low-temperature degeneracy 2. This agrees with the conjecture²³ that coherence effects are manifested below the coherence temperature T_k/N .

In conclusion, we have shown that the properties of CeAl₃, such as the inelastic neutron scattering spectra, the temperature dependence of the anisotropic static susceptibility, and specific heat above $T = 1$ K, can be described reasonably well by the single-impurity Anderson model with spin-orbit coupling and the hexagonal crystal field scheme proposed by Goremychkin *et al.*¹⁸ The fits to the high-temperature behavior indicate that any anisotropy in the hybridization is small. However, the calculations do not reproduce the small peak found in the $C(T)/T$ ratio at very low temperatures. This is presumably either due to coherence effects of the lattice or anomalous spin-glass-like ordering which has been proposed to occur in La-diluted CeAl₃.⁴

ACKNOWLEDGMENTS

This work was supported by the U.S. Department of Energy, Office of Basic Energy Science, Materials Science program.

¹P. W. Anderson, Phys. Rev. **126**, 41 (1961).

²P. Nozieres, J. Low Temp. Phys. **17**, 31 (1974).

³C. L. Lin, A. Wallash, J. E. Crow, T. Mihalisin, and P. Schlottmann, Phys. Rev. Lett. **58**, 1232 (1987).

⁴B. Andraka, C. S. Jee, and G. R. Stewart, Phys. Rev. B **52**, 9462 (1995).

⁵G. Lapertot, R. Calemczuk, C. Marcenat, J. Y. Henry, J. X. Boucherle, J. Flouquet, J. Hammann, R. Cibin, J. Cors, D. Jaccard, and J. Sierro, Physica B **186-188**, 454 (1993).

⁶S. Barth, H. R. Ott, F. N. Gygax, B. Hitti, E. Lippelt, A. Schenck, and C. Baines, Phys. Rev. B **39**, 11 695 (1989).

⁷W. H. Wong and W. G. Clark, J. Magn. Magn. Mater. **108**, 175 (1992).

⁸P. Nozieres, Ann. Phys. (Paris) **10**, 19 (1985); Eur. Phys. J. B **6**, 447 (1998).

⁹D. Jaccard, R. Cibin, A. Bezinge, J. Sierro, K. Matho, and J. Flouquet, J. Magn. Magn. Mater. **76&77**, 255 (1988).

¹⁰B. Coqblin and J. R. Schrieffer, Phys. Rev. **185**, 847 (1969).

¹¹E. A. Goremychkin, R. Osborn, B. D. Rainford, and A. P. Murani, Phys. Rev. Lett. **84**, 2211 (2000).

¹²T. A. Costi, Phys. Rev. Lett. **80**, 1038 (1998).

¹³R. Pietri, K. Ingersent, and B. Andraka, Phys. Rev. Lett. **86**, 1090

- (2001).
- ¹⁴Y. Kuramoto, *Z. Phys. B: Condens. Matter* **53**, 37 (1983).
- ¹⁵Y. Kuramoto and E. Müller-Hartmann, *J. Magn. Magn. Mater.* **52**, 122 (1985).
- ¹⁶N. E. Bickers, D. L. Cox, and J. W. Wilkins, *Phys. Rev. B* **36**, 2036 (1986).
- ¹⁷E. Segal and W. Wallace, *J. Solid State Chem.* **2**, 347 (1970).
- ¹⁸E. A. Goremychkin, R. Osborn, and I. L. Sashin, *J. Appl. Phys.* **85**, 6046 (1999).
- ¹⁹A. C. Hewson, *The Kondo Problem to Heavy Fermions* (Cambridge University Press, Cambridge, England, 1992).
- ²⁰E. Balcar and S. W. Lovesey, *J. Phys. C* **19**, 4605 (1986).
- ²¹A. P. Murani, K. Knorr, K. H. J. Buschow, A. Benoit, and J. Flouquet, *Solid State Commun.* **36**, 523 (1980).
- ²²P. M. Levy and S. Zhang, *Phys. Rev. Lett.* **62**, 78 (1989).
- ²³J. M. Lawrence, P. S. Riseborough, C. H. Booth, J. L. Sarrao, J. D. Thompson, and R. Osborn, *Phys. Rev. B* **63**, 054427 (2001).
- ²⁴A. N. Tahvildar-Zadeh, M. Jarrell, and J. Freericks, *Phys. Rev. B* **55**, R3332 (1997).
- ²⁵D. Cornut and B. Coqblin, *Phys. Rev. B* **5**, 4541 (1972).